RSC Advances

ROYAL SOCIETY OF CHEMISTRY

www.rsc.org/advances

Cite this: DOI: 10.1039/c0xx00000x

www.rsc.org/xxxxxx

ARTICLE TYPE

Electrocatalytic activity of Mn/Cu doped Fe_2O_3-PANI-rGO composites for Fuel cell applications

Karuppannan Mohanraju, Louis Cindrella*

Received (in XXX, XXX) Xth XXXXXXXXX 20XX, Accepted Xth XXXXXXXXX 20XX

DOI: 10.1039/b000000x

Low cost catalysts for oxygen reduction reaction (ORR) have been successfully synthesized from Mn/Cu doped Fe_2O_3-poly aniline (PANI) composite supported on reduced graphene oxide (rGO). The composite was prepared by oxidative polymerization followed by chemical reduction using hydrazine hydrate. Crystalline nature of Mn/Cu doped Fe_2O_3 was analyzed by X-ray diffraction (XRD) study. Surface morphology imaged by SEM shows the features of Mn/Cu doped Fe_2O_3 particles and PANI film on graphene sheets. The FT-IR studies revealed changes in the characteristic C-N and C=N stretching vibrations of PANI which confirmed that PANI was bonded to the surface of graphene sheets. Raman spectrum showed the presence of PANI on distorted graphene layers. TG/DTA studies revealed the thermal stability and extent of loading of Mn/Cu doped Fe_2O_3 in the composites. The electrocatalytic activity of the catalysts has been evaluated. Enhancements of ORR performance was observed in oxygen saturated 0.1 M KOH medium using the catalyst modified rotating disc electrode (RDE) and rotating ring disc electrode (RRDE). A maximum kinetic current density of -1.82 mA cm^{-2} at -0.2 V was obtained for Cu doped Fe_2O_3-PANI-rGO. Cu doped Fe_2O_3-PANI-rGO electrocatalyst has the Tafel slope of 156 mV dec^{-1}, onset potential of -46.4 mV and half wave potential of -225 mV. These values were obtained from ORR response at 1600 rpm. To the best of our knowledge, this is the first work to study the enhancements of ORR using Mn/Cu doped Fe_2O_3 and PANI on graphene support in alkaline medium. The durability studies showed that the synthesized electrocatalyst has better stability and also high methanol tolerance than the commercial 20 wt% Pt/C catalyst.

1. Introduction

Enormous research efforts are made for the development of non-precious catalysts to replace Pt as electrocatalyst in oxygen reduction reaction (ORR). Doped carbon catalysts are the most attractive for fuel cell applications favoring large scale commercialization of fuel cells by reducing the cost [1]. The research on non-precious catalysts was initiated by Jasinski using cobalt phthalocyanine [2] as ORR electrocatalyst. Later researchers replaced expensive macrocycle precursors with variety of inexpensive nitrogen containing chemicals like ammonia [3], amine [4] and amide [5]. They demonstrated that ORR active sites could be obtained by heat treatment of carbon along with nitrogen containing compounds [3-5]. Recently, nitrogen containing polymers are used as precursors to improve the activity of electrocatalyst [6]. Also the incorporation of non-precious metal (Co, Fe) [7]/ metal oxides (Fe_2O_3, Fe_3O_4, Co_3O_4) [8-10] has increased the active sites. Efficiency of the active sites varies with respect to method of synthesis, carbon sources, nitrogen sources and metals. It is reported that metal-nitrogen complex i.e., M-N_x (M = Co or Fe) is responsible for ORR activity of active sites [11]. But the M-N_x structure has the limitation of decomposing at higher temperature[12, 13] required for synthesizing N-doped carbon catalyst. In metal free N-doped carbon electrocatalyst, C-N active site is responsible for ORR [14], though the structure of ORR active sites and mechanism of ORR are still in controversial discussions [15, 16]. Chio et al. [17] prepared a series of catalysts of nitrogen-doped, carbon codoped with Fe, Co, Ni metal and investigated the effect of ORR activity with respect to various transition metals and reported the ORR activity in the order Co > Fe > Ni. Zhang et al. [18] synthesized a series of N-doped carbon based electrocatalysts with various transition metal codopants and reported the ORR activity in the order, Fe > Co > Zn > Mn > metal-free > Cu > Ni. The efficiency of each transition metal may relate to the active site structures and composition of catalysts. Other than transition metals, their oxides also increase the ORR activity of catalysts. Liang et al. [10] reported that Co_3O_4/N-graphene hybrid prepared by hydrothermal method showed enhanced catalytic activity and good stability in alkaline solution. Wu et al. [19] reported that the 3D monolithic Fe_3O_4/N-graphene aerogel hybrid exhibited high electrocatalytic activity for ORR and better stability in alkaline electrolyte. Nitrogen incorporation and metal oxide growth were achieved by hydrothermal method at 180 °C for 12 hours. In the present work, Mn/Cu doped Fe_2O_3 is used as metal oxide, PANI as nitrogen source and graphene as

the carbon source. We aim to synthesize the ORR active catalyst by refluxing the reactants and to study the effect of the synthesized bimetal oxide in ORR. Mn/Cu doped Fe_2O_3-PANI composites were characterized by XRD, SEM, FTIR, Raman spectrum and electrochemical methods. The XRD analysis of the composites confirms the presence of Mn/Cu doped Fe_2O_3, SEM - EDAX and elemental mapping images confirm the presence of Mn/Cu doped Fe_2O_3 particles and presence of PANI in composite, FT-IR data reveal the presence of PANI on graphene composites and Raman spectrum confirms the presence of well defined graphene sheets. The thermal analysis indicates the loading of bimetal oxides and the thermal stability of the composites. ORR activity and durability was examined in 0.1 M KOH electrolyte using rotating disc electrode (RDE). The kinetic parameters and ORR pathway are analyzed based on the obtained data.

2. Experimental

2.1. Synthesis of Mn/Cu doped Fe_2O_3-PANI Composites

Mn/Cu doped Fe_2O_3-PANI composites were synthesized by chemical oxidative method. Aniline was distilled prior to use. 25 ml of 0.2 M aniline, 2 ml of 0.2 M copper nitrate/manganese sulfate and 23 mL of 0.2 M ferric ammonium sulfate were mixed with 25 mL of 0.5 M KOH in a beaker. The solution was stirred well and maintained at 5 °C. 15 mL of 0.5 M ammonium persulfate was added gradually to the reaction mixture with constant stirring. pH was maintained at about 10 during the entire experiment. A dark green precipitate of PANI was obtained after 6 hours. The precipitate was filtered, washed with water several times and rinsed with acetone. Finally, it was dried at 60 °C for about 3 hours.

2.2. Synthesis of Mn/Cu doped Fe_2O_3-PANI-rGO Composite

Mn/Cu doped Fe_2O_3-PANI-rGO composites were prepared by reduction of graphene oxide along with Mn/Cu doped Fe_2O_3-PANI composites. Graphene oxide was synthesized by modified Hummer's method. 100 mL of water was taken in a round bottom flask and 60 mg of graphene oxide was dispersed in it by sonication. 40 mg of Mn/Cu doped Fe_2O_3-PANI was added to the flask and sonicated for 20 minutes. Reduction of graphene oxide was initiated by addition of 65 µL of hydrazine hydrate to the reaction mixture and by refluxing it for 12 hours. The precipitate formed was collected by ultracentrifugation, washed several times with water and dried at 60 °C.

2.3. Characterization techniques

The catalyst samples were studied by XRD technique (Rigaku Miniflex II Instrument) in the scattered angle range of 15° to 65° and in scan step of 2°/min using CuKα radiation (λ = 1.5406 Å). XRD analysis was carried out with 40 mg of catalyst spread uniformly over quartz plate. The morphological characterization and Energy dispersive X-ray analysis were carried out using EDAX coupled with HR-SEM instrument. The Raman spectra were recorded from Lab Raman HR Laser Raman Spectroscopy with sources of He-Ne (632 nm) and Ar (514 nm). FT-IR spectral analysis was carried out in JASCO-460 instrument in the frequency range of 4000 - 400 cm^{-1}. Electrochemical experiments were performed using an electrochemical workstation (Autolab PGSTAT302N), in a conventional three electrode system of Ag/AgCl as reference electrode, Pt mesh as counter electrode and 0.19625 cm^2 area of glassy carbon (GC) disc as working electrode. GC electrode was mirror polished with 0.05 micron alumina powder and cleaned well with Millipore water. 15 µL of catalyst in ethanol, absolute (Changshu Yangyuan Chemicals, china, purity 99.9 %) (5 mg per mL) was coated on GC by drop casting method, dried slowly at room temperature and then coated with Nafion film on the uniform surface of catalyst layer (3 µL of 0.05 wt% Nafion). Cyclic voltammetry studies were carried out in highly pure N_2 (INOX Nitrogen 5.0, purity 99.999%) and O_2 (INDO FAB, purity 99.98%) saturated 0.1 M KOH (Merck, India) solution in the potential window of -0.65 V to 1.20 V vs Ag/AgCl at a scan rate of 50 mV s^{-1}. Oxygen reduction studies were conducted by rotating disc electrode (RDE) technique in highly pure O_2 saturated 0.1 M KOH solution. Prepared electrodes were polarized negatively with potential from 0.20 to -0.65 V at a scan rate of 10 mV s^{-1}. Durability and methanol tolerance studies were carried out using chronoamperometric technique in presence of oxygen saturated 0.1 M KOH at constant potential of -0.3 V and with electrode rotation speed of 1600 rpm.

3. Results and Discussion

The crystallographic structure of Mn/Cu doped Fe_2O_3-PANI-rGO nanocomposite was analyzed by XRD (Fig. 1). A few characteristic peaks corresponding to (012), (104), (110), (113), (202), (024) and (116) planes were observed at $2\theta = 24.0^o$, 33.0^o, 35.5^o, 40.5^o, 43.5^o, 49.4^o and 53.9^o respectively. All these peaks were indexed to the rhombohedral structure of α- Fe_2O_3 and clearly matched with standard data file (JCPDS file no. 33-0664). XRD patterns indicated that Mn/Cu could be doping the lattice of the Fe_2O_3 without affecting rhombohedral structure [20, 21]. The characteristic peak at $2\theta = 25^o$ was due to 002 plane of the hexagonal structure of graphene nanosheets. The average crystallite size of Mn/Cu doped Fe_2O_3 was calculated from the first three high intensity XRD patterns using Scherrer equation. $Mn_xFe_{2-x}O_3$ and $Cu_xFe_{2-x}O_3$ showed average crystallite size as 13±1 nm and 14±2 nm respectively. Inset of Fig. 1 (XRD patterns for graphite and graphite oxide) shows the conversion of graphite to graphite oxide by Hummers method.

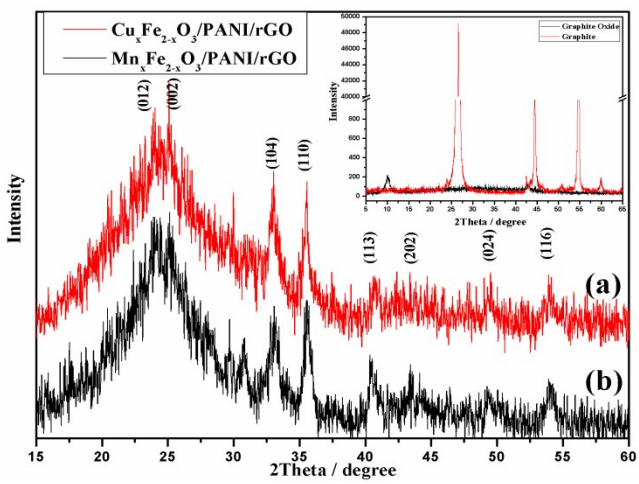

Fig. 1. XRD patterns of Mn/Cu doped Fe_2O_3-PANI-rGO composites, (Insets for graphite and graphite oxide)

Cite this: DOI: 10.1039/c0xx00000x

www.rsc.org/xxxxxx

ARTICLE TYPE

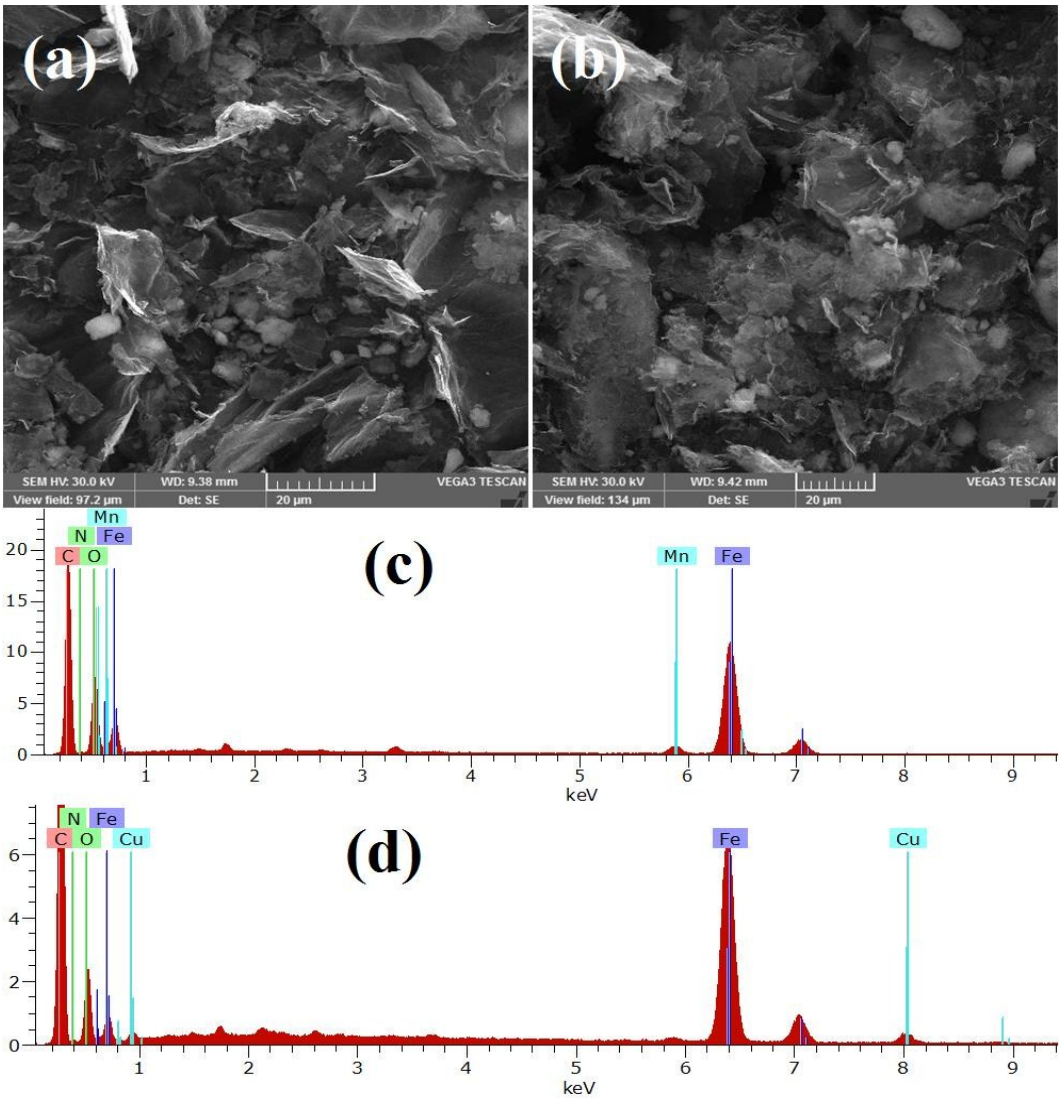

Fig. 2. SEM and EDAX spectrum of Mn doped Fe_2O_3-PANI-rGO (a, c), Cu doped Fe_2O_3-PANI-rGO (b, d) composites.

Fig. 2 shows the surface morphology of Mn doped Fe_2O_3-PANI-rGO composite (a) and Cu doped Fe_2O_3-PANI-rGO (b) composite. The selected area of composites is further analyzed by EDAX. EDAX spectrum of Mn doped Fe_2O_3-PANI-rGO (Fig. 2c) composite reveals the presence of carbon, oxygen, nitrogen, iron and manganese in the weight ratio of 50.4:33.6:3.9:11.5:0.6. Cu doped Fe_2O_3-PANI-rGO (Fig. 2d) composite shows carbon, oxygen, nitrogen, iron and copper in the weight ratio of 63.2:20.5:3.5:11.9:0.9. The SEM image and EDAX images clearly show that Mn/Cu doped Fe_2O_3 particles along with PANI films cover the graphene sheets. Fig. S1 SEM image and elemental mapping of Mn doped Fe_2O_3-PANI-rGO (a), Cu doped Fe_2O_3-PANI-rGO (b) show the uniform distribution of Mn/Cu doped Fe_2O_3 particles and PANI on the graphene sheets in the composites. Elemental mapping images are given on the right side of the SEM image. Each element is shown in different color i.e. Carbon, nitrogen, oxygen, iron are identified in light turquoise, pink, blue and green colors respectively, and copper and manganese are identified in red color.

The composites were further analyzed by FT-IR spectroscopy to identify the nature of bonding present in the composites. Fig. 3a shows the FT-IR spectra of rGO and Mn/Cu doped Fe_2O_3-PANI-rGO composites. Spectrum of rGO reveals the peaks around 1742 cm^{-1} for stretching vibrations of C=O in COOH group, 1634 cm^{-1} for O-H stretching vibrations of intercalated water and 1404-1051 cm^{-1} due to C-O stretching vibrations in alkoxy/epoxy functional groups [22-24]. When compared with rGO, Mn/Cu doped Fe_2O_3-PANI-rGO composites show additional peaks at about

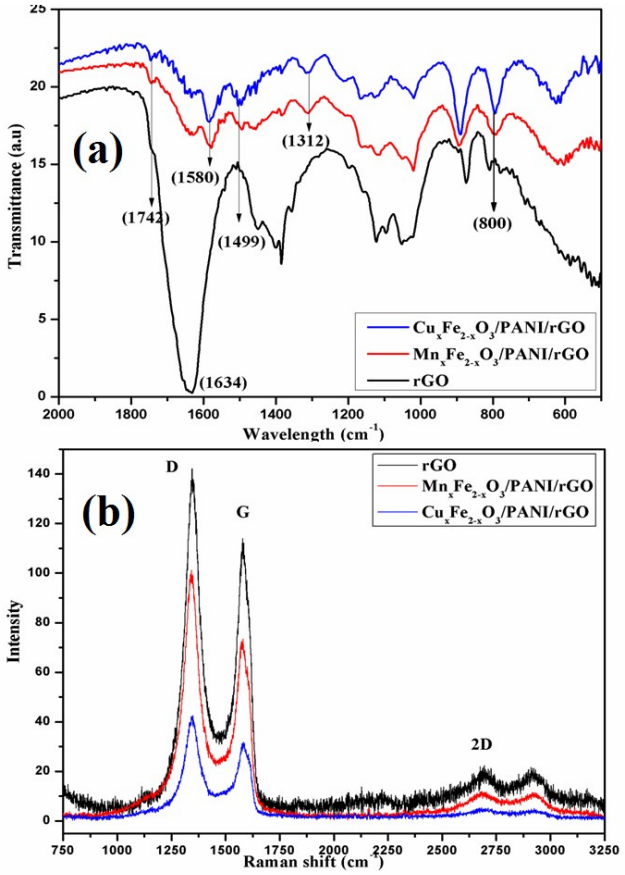

Fig. 3. (a) FT-IR and (b) Raman spectra of as synthesized rGO, Mn/Cu doped Fe_2O_3-PANI-rGO composites.

1580 cm^{-1}, 1499 cm^{-1} due to C=N and C=C stretching of the quinonoid and benzenoid units respectively. Peak at 1312 cm^{-1} is due to C-N stretching [25]. The peak at 800 cm^{-1} is attributed to C-H out of plane bending vibration. There are many low intensity peaks in the range of 780 - 580 cm^{-1} responsible for C-H bonds of the benzene rings. Peaks corresponding to the C=N and C-N stretching vibrations confirm the presence of PANI in Mn/Cu doped Fe_2O_3-PANI-rGO composites. Raman spectroscopy is a non-destructive tool to analyze the microstructure of carbon materials. Fig. 3b shows that Raman spectra of rGO, Mn/Cu doped Fe_2O_3-PANI-rGO composites display two predominant peaks at 1342 and 1578 cm^{-1} corresponding to the D and G bands respectively. D band is assigned to the breathing mode of k-point phonons of A_{1g} symmetry with vibrations of the carbon atoms of the disordered and defected graphite. G band is related to E_{2g} phonons of sp^2 carbon atoms [26-28]. The intensity ratio of D/G band is 1.26, 1.40, 1.34 for rGO, Mn doped Fe_2O_3-PANI-rGO and Cu doped Fe_2O_3-PANI-rGO respectively which are higher than those of graphite oxide and commercial graphite reported in literature [29]. D/G band intensity ratio of Mn/Cu doped Fe_2O_3-PANI-rGO composites shows higher value than rGO indicating an increased defects or edge areas in carbon structures. Other than D and G bands, the 2D band is observed at about 2700 cm^{-1} in Fig. 3b. It has been recently reported [28] that the shape and position of the 2D band explain the number of the layers in the graphene sheets and the 2D peak position of single layer graphene sheet occurred at 2679 cm^{-1}, while 2D band of multilayer (2-4 layers) displayed frequency at 19 cm^{-1} higher. In our work, the 2D peak appears at 2689 cm^{-1} revealing that less than four layers of graphene sheets may have been formed.

The comparison of mass loss on heating in presence of nitrogen and air would explain the thermal stability and metal oxide loading in composites respectively. Fig. 4a shows the thermo grams of rGO and Mn/Cu doped Fe_2O_3-PANI-rGO composites in nitrogen atmosphere. The initial mass loss in the range of 100 to 150 ^oC is due to the deintercalation of H_2O [30]. In composites, PANI starts to decompose from 230 ^oC, which agreed with the results of previous report [31] for PANI-rGO composites. The mass loss of PANI is higher in Cu doped Fe_2O_3-PANI-rGO composite (5.5 %) than Mn doped Fe_2O_3-PANI-rGO composite (3.2 %). Beyond 230 ^oC the composites containing Mn/Cu doped Fe_2O_3-rGO only show mass change due to defects characteristic of rGO [32] at about 500-600 ^oC. The defect formation occurs at 620 ^oC in rGO and at about 550 ^oC in Mn/Cu doped Fe_2O_3-rGO. Graphene structures in rGO decomposed from 900 ^oC but Mn/Cu doped Fe_2O_3-PANI-rGO composite graphene structures started to decompose from 842 ^oC and 770 ^oC respectively. The metal oxides act as oxygen source for rGO in nitrogen atmosphere allowing the decomposition of rGO in composites at relatively lower temperature than pristine rGO. The loading of Mn/Cu doped Fe_2O_3 was determined from TG/DTA analysis in presence of air atmosphere. Fig 4b shows loading of Mn doped Fe_2O_3 as 7 wt % and Cu doped Fe_2O_3 as 13.2 wt % in their respective composites. DTA curve reveals maximum change in mass occurring at 497 ^oC for Cu doped Fe_2O_3-PANI-rGO and 547 ^oC

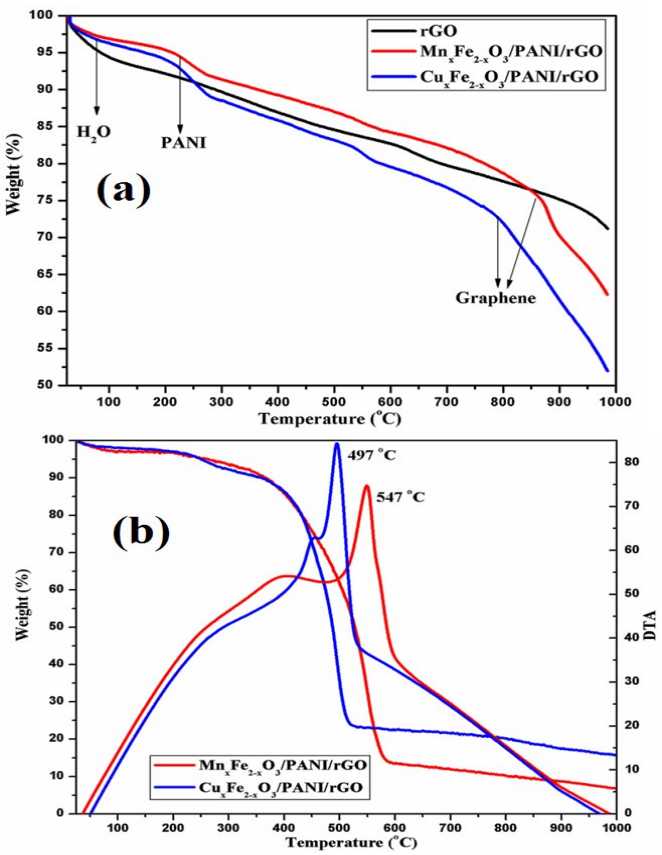

Fig. 4. Thermogravimetric plots of (a) rGO, Mn/Cu doped Fe_2O_3-PANI-rGO composites in N_2 atmosphere, (b) TG and DTA plots of Mn/Cu doped Fe_2O_3-PANI-rGO composites in air atmosphere.

Cite this: DOI: 10.1039/c0xx00000x

www.rsc.org/xxxxxx

ARTICLE TYPE

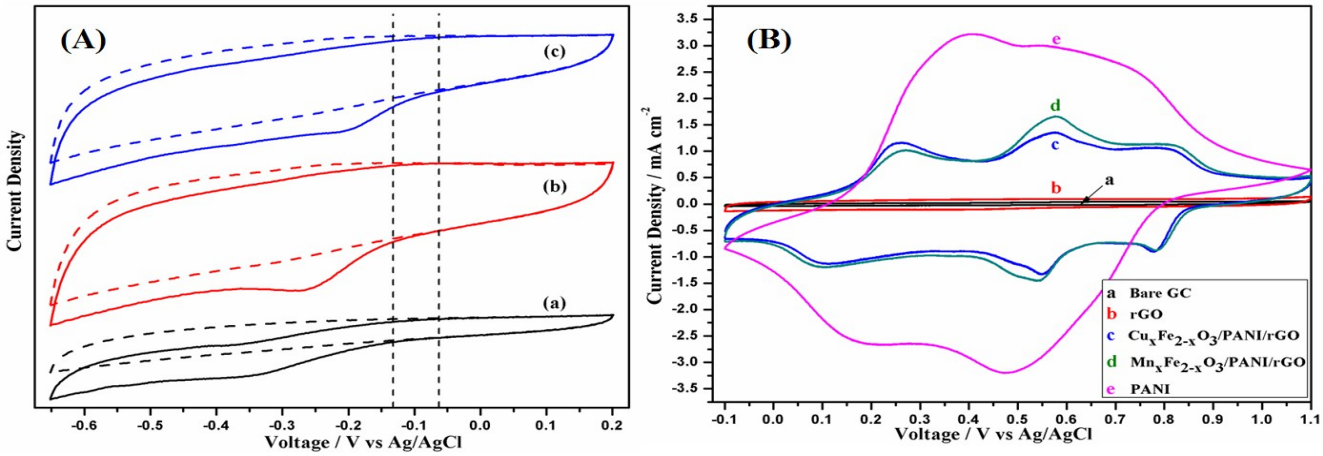

Fig. 5A. Cyclic voltammetry curves of (a) rGO, (b) Mn doped Fe_2O_3-PANI-rGO and (c) Cu doped Fe_2O_3-PANI-rGO in presence of nitrogen (dashed line) and saturated oxygen (solid line) in 0.1 M KOH electrolyte at 50 mV s^{-1}. Fig. 5B. CV curves of bare GC, rGO, Mn/Cu doped Fe_2O_3-PANI-rGO, PANI in 1 M H_2SO_4 at a scan rate of 100 mV s^{-1}

for Mn doped Fe_2O_3-PANI-rGO composites. Thus it can be inferred that the thermal stability of the composites depend on the Mn/Cu doped Fe_2O_3 content.The deviation in thermal stability of the composites could be observed in the metal oxide loaded composites. The thermograms reveal that increasing metal oxide loading in graphene composites reduced the thermal stability of the composites compared to that rGO.

The electrocatalytic activity of as synthesized rGO and Mn/Cu doped Fe_2O_3-PANI-rGO composites were characterized by cyclic voltammetry (CV). Fig. 5A shows CV curves recorded in 0.1 M KOH electrolyte in the potential range of -0.65 to 0.20 V at scan rate of 50 mV s^{-1} in presence of saturated O_2 and N_2 atmosphere.

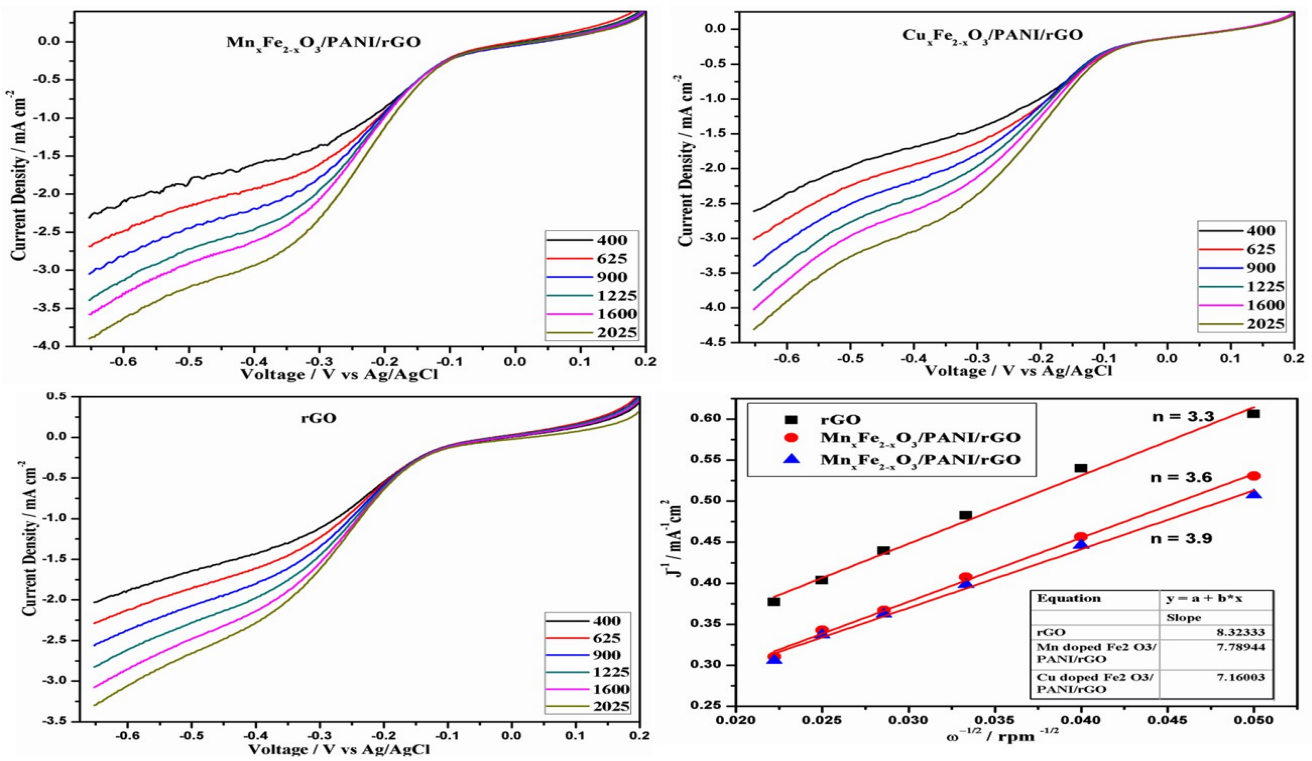

Fig. 6. Linear polarization curves of Mn/Cu doped Fe_2O_3-PANI-rGO, rGO electrocatalysts in O_2-saturated 0.1 M KOH at a scan rate of 10 mV s^{-1} recorded at various rotation rate. K-L plots of rGO, Mn/Cu doped Fe_2O_3-PANI-rGO electrocatalysts at -0.4 to -0.6V

Cite this: DOI: 10.1039/c0xx00000x

www.rsc.org/xxxxxx

ARTICLE TYPE

Table 1. K-L slope, number of electrons (n), kinetic current density (j_K), Tafel slope (mV dec^{-1}), onset potential and half wave potentials ($E_{1/2}$) of rGO, Mn/Cu doped Fe_2O_3-PANI-rGO.

Electrocatalysts	K-L Slope (mA^{-1} cm^2 $rpm^{1/2}$)	n	Jk (mA cm^{-2})	Tafel slope (mV dec^{-1})	Onset potential (mV)	$E_{1/2}$ (mV)
rGO	8.3	3.4	-0.91	127	-108	-288
$Mn_x Fe_{2-x}O_3$-PANI-rGO	7.9	3.6	-1.45	151	-73.2	-241
$Cu_x Fe_{2-x}O_3$-PANI-rGO	7.2	3.9	-1.82	156	-46.4	-225
Pt/C	7.2	3.9	-11.5	106	15.0	-126

rGO, Mn/Cu doped Fe_2O_3-PANI-rGO electrocatalysts clearly show their oxygen reduction ability in the presence of saturated oxygen medium as contrasted with that in nitrogen. Similar trends for N-doped materials has also been reported [33]. The onset potential of Mn/Cu doped Fe_2O_3-PANI-rGO electrocatalysts showed 70 mV and 33 mV higher potential than that of rGO respectively. It confirms that Mn/Cu doped Fe_2O_3-PANI-rGO composites have better electrocatalytic activity than rGO. Cyclic voltammetry studies are also helpful to identify the presence of PANI in Mn/Cu doped Fe_2O_3-PANI-rGO composites. Electrochemical response of bare GC, rGO, Mn/Cu doped Fe_2O_3-PANI-rGO, PANI are evaluated in 1 M H_2SO_4 in the potential range of -0.1 V to 1.1 V Vs. Ag/AgCl (Fig. 5B). CV curves clearly show that there is no peak obtained for bare GC and rGO. Mn/Cu doped Fe_2O_3-PANI-rGO show redox peaks similar to pure PANI [25, 34]. This confirms the presence of PANI thin layer in electrochemical active surface of Mn/Cu doped Fe_2O_3-PANI-rGO electrodes.

Oxygen reduction activity of the electrocatalysts synthesized are further characterized by linear polarization of rotating disc electrode (RDE) with a scan rate of 10 mV s^{-1} in oxygen saturated 0.1 M KOH electrolyte. Fig. 6 reveals well defined oxygen reduction curves with respect to various rotations in the potential window of 0.20 to -0.65 V. The electrocatalytic efficiency was determined by identifying the mechanism of ORR using Koutecky - Levich (K-L) equation [35]. The measured current density (j) is related to kinetic current density (j_K) and limiting current density (j_L) by the K-L equation as represented below.

$$1/j = 1/j_K + 1/j_L \quad \ldots \quad (1)$$

Where $j_K = nFkCo_2$

$$J_L = 0.2nFACo_2 (Do_2)^{2/3} \nu^{-1/6} \omega^{1/2}$$

n is number of electrons, F is Faraday constant, k is electron transfer rate constant, A is area of the working electrode, Co_2 is concentration of dissolved oxygen, Do_2 is diffusion coefficient of O_2 in 0.1 M KOH electrolyte, ν is kinematic viscosity of the electrolyte, ω is speed of the electrode in revolution per minute (rpm) [36, 37]. The K-L plot of j^{-1} Vs $\omega^{-1/2}$ at fixed potential (-0.5 V) in limiting current density region gives a straight line which indicates the first order kinetics with respect to molecular oxygen. Number of electrons involved in the ORR is calculated from the slope of the straight line obtained in the K-L plots. The value of 'n' obtained for rGO, Mn doped Fe_2O_3-PANI-rGO and Cu doped Fe_2O_3-PANI-rGO at potential values of -0.5 V are 3.3, 3.6 and 3.9 respectively. The 'n' value closer to 4 indicates that water is the main product and not hydrogen peroxide. Hence the tendency for water formation [38] decreased in the order, Cu doped Fe_2O_3-PANI-rGO > Mn doped Fe_2O_3-PANI-rGO > rGO. Cu doped Fe_2O_3-PANI-rGO electrocatalysts follow four electron transfer mechanism in ORR. The ORR activity of as synthesized catalysts is analyzed by RRDE in presence of saturated O_2 in the potential window of 0.2 to -0.7 V with a scan rate of 10 mV s^{-1}. Number of electrons was calculated using the following equation.

$$n = 4I_D / [I_D + (I_R/CE)] \quad \ldots \quad (2)$$

Where, I_D is disc current, I_R is ring current; CE is collection efficiency of ring electrode. Number of electron involved in ORR was calculated for rGO, Mn doped Fe_2O_3-PANI-rGO, and

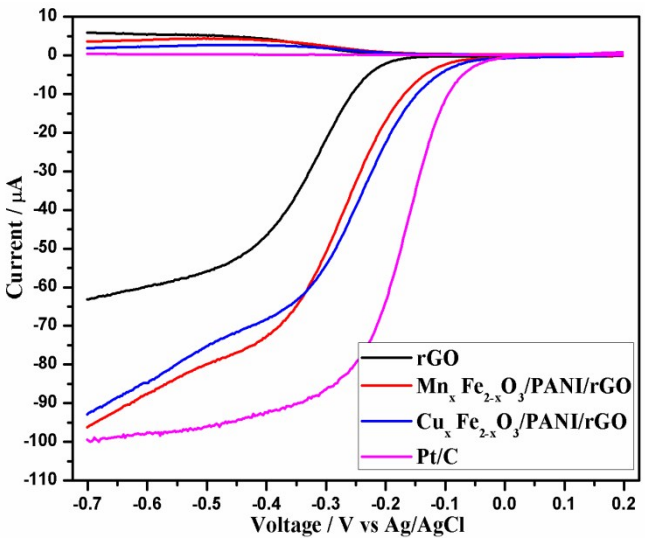

Fig. 7. Rotating ring disc voltammograms of rGO, Mn/Cu doped Fe_2O_3-PANI-rGO and Pt/C electrodes at rotation rate of 1600 rpm in O_2 saturated 0.1 M KOH at a scan rate of 10 mV s^{-1}.

Cite this: DOI: 10.1039/c0xx00000x

www.rsc.org/xxxxxx

ARTICLE TYPE

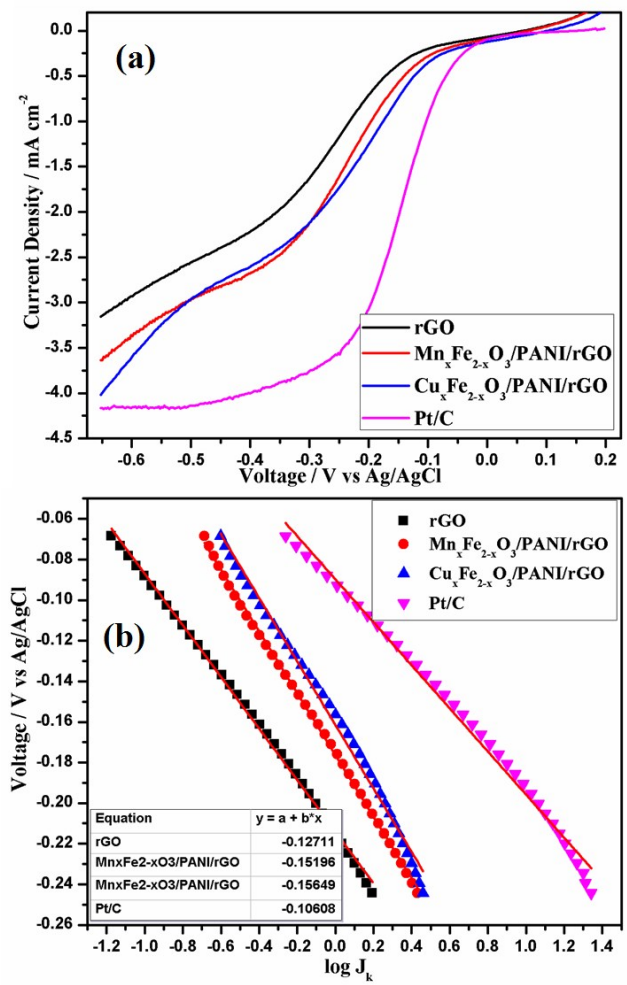

Fig. 8. a) Rotating-disc voltammograms of rGO, Mn/Cu doped Fe_2O_3-PANI-rGO and Pt/C electrodes at rotation rate of 1600 rpm in O_2 saturated 0.1 M KOH at a scan rate of 10 mV s^{-1}. b) Tafel slopes of rGO, Mn/Cu doped Fe_2O_3-PANI-rGO and Pt/C electrocatalysts.

Cu doped Fe_2O_3-PANI-rGO and Pt/C as 3.2, 3.5, 3.7 and 3.9 respectively at fixed potential of -0.6 V. Ring current is the response of hydrogen peroxide reduction. The efficiency of electrocatalysts for ORR are listed in order of ring current response and calculated n values as Pt/C > Cu doped Fe_2O_3-PANI-rGO > Mn doped Fe_2O_3-PANI-rGO > rGO. Fig S2 – S6 show the rotating ring disc voltammograms of Pt/C, Mn/Cu doped Fe_2O_3-PANI-rGO, rGO electrodes in O_2-saturated 0.1 M KOH at a scan rate of 10 mV s^{-1} recorded at various rotation rates.

$$J_K = J*J_L/J_L-J \quad \ldots \quad (3)$$

Using the equation 3, The kinetic current density (J_k) of rGO and Mn/Cu doped Fe_2O_3-PANI-rGO and Pt/C electrocatalysts are -0.91, -1.45, -1.82, and -11.5 mA cm^{-2} respectively which are calculated at low current density region at -0.2 V (Fig. 8a).The ORR performance of as synthesized catalysts evaluated at 1600 rpm at scan rate of 10 mV s^{-1}. Onset potential value of rGO, Mn/Cu doped Fe_2O_3-PANI-rGO and Pt/C are -108, -73.2, -46.4 and 15 mV respectively. The half wave potential of rGO, Mn/Cu doped Fe_2O_3-PANI-rGO and Pt/C are -288, -241, -225 and -126 mV respectively. The half wave potential ($E_{1/2}$) of Cu doped Fe_2O_3-PANI-rGO is 16 mV higher than Mn doped Fe_2O_3-PANI-rGO and 63 mV higher than rGO. While comparing commercial Pt/C, Mn doped Fe_2O_3-PANI-rGO has 115 mV lower $E_{1/2}$ value and Cu doped Fe_2O_3 has 99 mV lower $E_{1/2}$ value. Previous reports for (N or S) doped graphene electrocatalysts showed half wave potential value less than -0.25 V in alkaline electrolytes which are lesser than Mn/Cu doped Fe_2O_3-PANI-rGO electrocatalyst[39, 40]. It clearly shows that ORR activity of the catalysts is in the order, Pt/C > Cu doped Fe_2O_3-PANI-rGO > Mn doped Fe_2O_3-PANI-rGO > rGO. The homogeneity of the platinum surface facilitates uniform adsorption of the species and isotropic electroactivity which results in diffusion limited current density. Whereas the heterogeneity of the Mn/Cu doped Fe_2O_3-PANI-rGO composites have anisotropic active sites which behave differently at different applied potential thereby exhibiting electroactivity continuously at one site or the other which is the reason for the current density not limited by diffusion. Reports [41, 42] also reveal that N-doped graphene electrocatalysts are having higher diffusion limiting current densities.

The kinetics of the ORR was analyzed from the mass transport corrected Tafel plots of the synthesized electrocatalysts. rGO, Mn/Cu doped Fe_2O_3-PANI-rGO show Tafel slope values of 127, 151 and 156 mV dec^{-1} respectively. While comparing with rGO, Mn/Cu doped Fe_2O_3-PANI-rGO composites have deviations in the Tafel slope values which could have occurred by adsorption of oxygenated species on surface of the active centers. Though previous reports for platinum based electrocatalysts [43] generally showed Tafel slope around 120 mV dec^{-1} in high current density region, higher values of about 200 mV dec^{-1} have also been reported for Pt/CNT modified electrode in high current density region [44]. rGO, Mn/Cu doped Fe_2O_3-PANI-rGO electrodes also exhibited Tafel slope values in the range reported for Pt based electrocatalysts. Tafel results are given in Table 1. At high current density region, the Tafel slopes of electrocatalysts such as Fc-NCNT, FePc-NCNT have been reported [45] to be 136 and 171 mV dec^{-1} respectively and these results are almost in the same range as those of Mn/Cu doped Fe_2O_3-PANI-rGO electrocatalysts of our study. As the Tafel slope of 120 mV dec^{-1} has also been reported for adsorption of O_2 on platinum electrocatalysts by Langmuir adsorption isotherm [43], the values obtained for the electrocatalysts synthesized in this study are indicative of similar adsorption mechanism during ORR process. The results obtained from ORR experiments such as K-L slope, number of electrons,

kinetic current density, Tafel slope, onset potential and half wave potentials of rGO, Mn/Cu doped Fe_2O_3-PANI-rGO are listed in Table 1.

The durability of as synthesized electrocatalyst was examined by chronoamperometric response under constant cathodic voltage of -0.3 V for 5000 seconds in O_2 saturated 0.1 M KOH electrolyte. As shown in Fig. 9a, the current decay measured for Pt/C, Mn/Cu doped Fe_2O_3-PANI-rGO is 47.6, 36.6 and 33.5 % respectively. The results clearly reveal that the order of stability is Cu doped Fe_2O_3-PANI-rGO > Mn doped Fe_2O_3-PANI-rGO > Pt/C. PANI

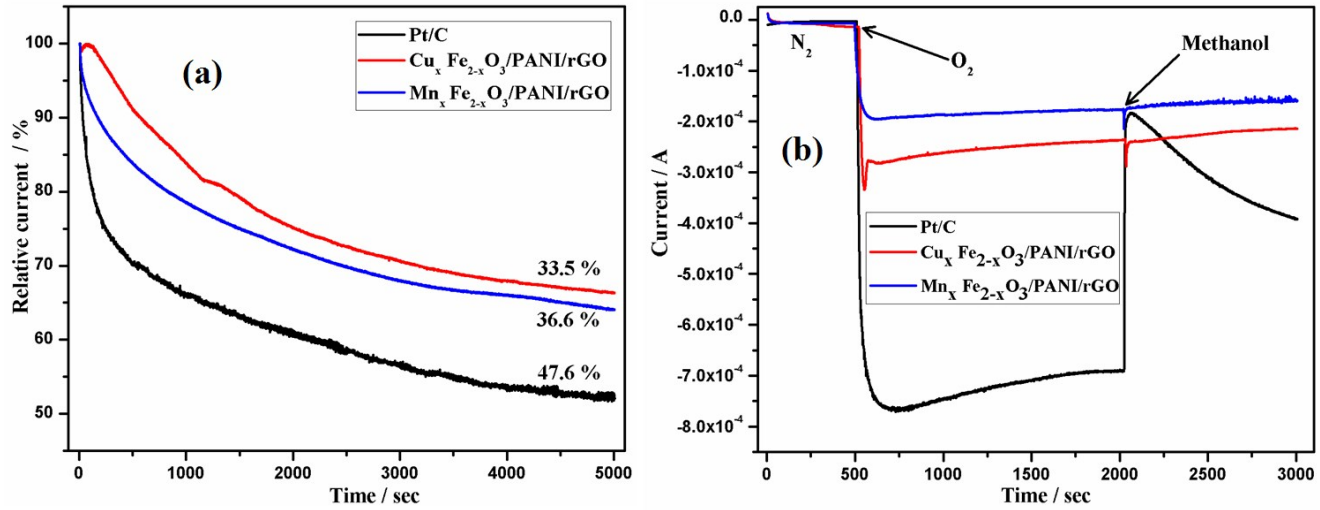

Fig. 9a. Chronoamperometric response of Mn/Cu doped Fe_2O_3-PANI-rGO and Pt/C at -0.3 V in O_2 saturated 0.1 M KOH solution at a rotation rate of 1600 rpm. Fig. 9b. Methanol crossover study of Mn/Cu doped Fe_2O_3-PANI-rGO and Pt/C at a rotation speed of 1600 rpm. At 2000 s 3 M methanol was added into the O_2 saturated 0.1 M KOH electrolyte to evaluate the crossover effect.

based graphene composites possess better stability than Pt/C. Mn/Cu doped Fe_2O_3-PANI-rGO electrodes are further subjected to methanol cross over test which is helpful to study the ORR in presence of other fuel like methanol. Fig. 9b shows the chronoamperometric response of Mn/Cu doped Fe_2O_3-PANI-rGO and Pt/C with respect to N_2, O_2 and O_2 with 3 M methanol at a speed of 1600 rpm. At constant potential (-0.3 V), ORR response of Cu doped Fe_2O_3-PANI-rGO is higher than that of Mn doped Fe_2O_3-PANI-rGO while Pt/C scored higher than the other two even after addition of methanol. When adding 3M methanol to O_2 saturated 0.1 M KOH electrolyte under chronoamperometric conditions, the disturbance in ORR is higher in the case of Pt/C than that of Mn/Cu doped Fe_2O_3-PANI-rGO. Mn/Cu doped Fe_2O_3-PANI-rGO electrocatalysts showed similar ORR stability in the presence of methanol. The reported catalysts are more tolerant to the presence of methanol than Pt/C.

4. Conclusion

A simple and low cost method is reported for the synthesis of Mn/Cu doped Fe_2O_3-PANI-rGO electrocatalysts and they have been demonstrated as catalysts for ORR. The structural, morphological and thermal stability properties have been deduced from XRD, HR SEM, FT-IR, Raman spectra and TG/DTA analysis. The ORR activity was evaluated by RDE and RRDE techniques in O_2 saturated alkaline medium. K-L slopes proved that the hydrogen peroxide by product formation using Cu doped Fe_2O_3-PANI-rGO was lesser than Mn doped Fe_2O_3-PANI-rGO and rGO, and it follows four electron transfer pathway mechanism. Kinetic paramenters such as Tafel slope values are closer to 120 mV dec^{-1} and indicative of one electron transfer as the rate determining step and Langmuir adsorption isotherm as the adsorption mechanism. The kinetic current density, onset potential and half wave potential values were calculated which confirmed that Mn/Cu doped Fe_2O_3-PANI-rGO electrodes have better ORR activity than rGO. The order of ORR activity is, Cu doped Fe_2O_3-PANI-rGO > Mn doped Fe_2O_3-PANI-rGO > rGO. Durability and methanol tolerance studies of as synthesized electrocatalysts were carried out and compared with commercial Pt/C (20 wt %), which proved better durability than Pt/C.

Acknowledgment

The authors acknowledge the financial support from MHRD, India through lab facilities and fellowship.

Notes

Fuel Cell lab, Department of Chemistry, National Institute of Technology, Tiruchirappalli - 620015, India. Fax: +91 431 2500133; Tel: +91 431 2503634; Email: cind@nitt.edu

† Electronic Supplementary Information (ESI) available: [Elemental mapping images of Mn doped Fe_2O_3-PANI-rGO (a), Cu doped Fe_2O_3-PANI-rGO (b) composites. RRDE studies of rGO, Pt/C, Mn/Cu doped Fe_2O_3-PANI-rGO composites]. See DOI: 10.1039/b000000x/

Reference

1. M. K. Debe, *Nature*, 2012, **486**, 43-51.
2. R. Jasinski, *Nature*, 1964, **201**, 1212-1213.
3. X. Wang, X. Li, L. Zhang, Y. Yoon, P. K. Weber, H. Wang, J. Guo and H. Dai, *Science*, 2009, **324**, 768-771.
4. Z.-H. Sheng, L. Shao, J.-J. Chen, W.-J. Bao, F.-B. Wang and X.-H. Xia, *ACS Nano*, 2011, **5**, 4350-4358.
5. Z. Lin, G. Waller, Y. Liu, M. Liu and C.-P. Wong, *Advanced Energy Materials*, 2012, **2**, 884-888.
6. G. Wu, K. L. More, C. M. Johnston and P. Zelenay, *Science*, 2011, **332**, 443-447.

7. X. Fu, Y. Liu, X. Cao, J. Jin, Q. Liu and J. Zhang, *Appl. Catal. B: Environ.*, 2013, **130–131**, 143-151.
8. C. H. Choi, S. Y. Lee, S. H. Park and S. I. Woo, *Appl. Catal. B: Environ.*, 2011, **103**, 362-368.
9. Y. Ye, L. Kuai and B. Geng, *J. Mater. Chem.*, 2012, **22**, 19132-19138.
10. Y. Liang, Y. Li, H. Wang, J. Zhou, J. Wang, T. Regier and H. Dai, *Nat. Mater.*, 2011, **10**, 780-786.
11. R. Bashyam and P. Zelenay, *Nature*, 2006, **443**, 63-66.
12. K. Wiesener, *Electrochim. Acta*, 1986, **31**, 1073-1078.
13. E. Yeager, *Electrochim. Acta*, 1984, **29**, 1527-1537.
14. Y. Ma, L. Sun, W. Huang, L. Zhang, J. Zhao, Q. Fan and W. Huang, *J. Phys. Chem. C*, 2011, **115**, 24592-24597.
15. Z. Chen, D. Higgins, A. Yu, L. Zhang and J. Zhang, *Energy Environ. Sci.*, 2011, **4**, 3167-3192.
16. C. W. B. Bezerra, L. Zhang, K. Lee, H. Liu, A. L. B. Marques, E. P. Marques, H. Wang and J. Zhang, *Electrochim. Acta*, 2008, **53**, 4937-4951.
17. C. H. Choi, S. H. Park and S. I. Woo, *Appl. Catal. B: Environ.*, 2012, **119–120**, 123-131.
18. H.-J. Zhang, Q.-Z. Jiang, L. Sun, X. Yuan, Z. Shao and Z.-F. Ma, *Int. J. Hydrogen Energy*, 2010, **35**, 8295-8302.
19. Z.-S. Wu, S. Yang, Y. Sun, K. Parvez, X. Feng and K. Müllen, *J. Am. Chem. Soc.*, 2012, **134**, 9082-9085.
20. P. Sun, C. Wang, X. Zhou, P. Cheng, K. Shimanoe, G. Lu and N. Yamazoe, *Sens. Actuators B*, 2014, **193**, 616-622.
21. H.-J. Cui, J.-K. Cai, J.-W. Shi, B. Yuan, C.-L. Ai and M.-L. Fu, *RSC Adv.*, 2014, **4**, 10176-10179.
22. H. Wang, Q. Hao, X. Yang, L. Lu and X. Wang, *Electrochem. Commun.*, 2009, **11**, 1158-1161.
23. S. Park, K.-S. Lee, G. Bozoklu, W. Cai, S. T. Nguyen and R. S. Ruoff, *ACS Nano*, 2008, **2**, 572-578.
24. A. Dato, Z. Lee, K.-J. Jeon, R. Erni, V. Radmilovic, T. J. Richardson and M. Frenklach, *Chem. Commun.*, 2009, 6095-6097.
25. J. Xu, K. Wang, S.-Z. Zu, B.-H. Han and Z. Wei, *ACS Nano*, 2010, **4**, 5019-5026.
26. Y. Liu, R. Deng, Z. Wang and H. Liu, *J. Mater. Chem.*, 2012, **22**, 13619-13624.
27. H.-L. Guo, X.-F. Wang, Q.-Y. Qian, F.-B. Wang and X.-H. Xia, *ACS Nano*, 2009, **3**, 2653-2659.
28. O. Akhavan, *Carbon*, 2010, **48**, 509-519.
29. X. Lu, H. Dou, S. Yang, L. Hao, L. Zhang, L. Shen, F. Zhang and X. Zhang, *Electrochim. Acta*, 2011, **56**, 9224-9232.
30. S. Liu, X. Liu, Z. Li, S. Yang and J. Wang, *New J. Chem.*, 2011, **35**, 369-374.
31. Y. Du, S. Z. Shen, W. Yang, R. Donelson, K. Cai and P. S. Casey, *Synth. Met.*, 2012, **161**, 2688-2692.
32. H. Y. Nan, Z. H. Ni, J. Wang, Z. Zafar, Z. X. Shi and Y. Y. Wang, *Journal of Raman Spectroscopy*, 2013, **44**, 1018-1021.
33. H. Wang, T. Maiyalagan and X. Wang, *ACS catal.*, 2012, **2**, 781-794.
34. N. A. Kumar, H.-J. Choi, Y. R. Shin, D. W. Chang, L. Dai and J.-B. Baek, *ACS Nano*, 2012, **6**, 1715-1723.
35. K. Mohanraju and L. Cindrella, *RSC Adv.*, 2014, **4**, 11939-11947.
36. S. M. Unni, S. Devulapally, N. Karjule and S. Kurungot, *J. Mater. Chem.*, 2012, **22**, 23506-23513.
37. B. J. Kim, D. U. Lee, J. Wu, D. Higgins, A. Yu and Z. Chen, *J. Phys. Chem. C*, 2013, **117**, 26501-26508.
38. K. Lee, L. Zhang, H. Lui, R. Hui, Z. Shi and J. Zhang, *Electrochim. Acta*, 2009, **54**, 4704-4711.
39. L. Qu, Y. Liu, J.-B. Baek and L. Dai, *ACS Nano*, 2010, **4**, 1321-1326.
40. S. Yang, L. Zhi, K. Tang, X. Feng, J. Maier and K. Müllen, *Advanced Functional Materials*, 2012, **22**, 3634-3640.
41. Y. Ma, L. Sun, W. Huang, L. Zhang, J. Zhao, Q. Fan and W. Huang, *The Journal of Physical Chemistry C*, 2011, **115**, 24592-24597.
42. K. Parvez, S. Yang, Y. Hernandez, A. Winter, A. Turchanin, X. Feng and K. Müllen, *ACS Nano*, 2012, **6**, 9541-9550.
43. H. A. Gasteiger and P. N. Ross, *J. Phys. Chem. C*, 1996, **100**, 6715-6721.
44. N. Alexeyeva, K. Tammeveski, A. Lopez-Cudero, J. Solla-Gullón and J. M. Feliu, *Electrochim. Acta*, 2010, **55**, 794-803.
45. Z. Chen, D. Higgins and Z. Chen, *Electrochim. Acta*, 2010, **55**, 4799-4804.